Journal of Geophysical Research: Oceans

RESEARCH ARTICLE
10.1029/2018JC013797

Special Section:
Sea State and Boundary Layer Physics of the Emerging Arctic Ocean

Stable Isotope Clues to the Formation and Evolution of Refrozen Melt Ponds on Arctic Sea Ice

L. Tian[1], Y. Gao[1], S. F. Ackley[1], S. Stammerjohn[2], T. Maksym[3], and B. Weissling[1]

[1]Center for Water Research, Department of Geological Sciences, University of Texas at San Antonio, San Antonio, TX, USA, [2]Institute of Arctic and Alpine Research, University of Colorado Boulder, Boulder, CO, USA, [3]Woods Hole Oceanographic Institution, Woods Hole, MA, USA

Abstract Sea ice is one of the determining parameters of the climate system. The presence of melt ponds on the surface of Arctic sea ice plays a critical role in the mass balance of sea ice. A total of nine cores was collected from multiyear ice refrozen melt ponds and adjacent hummocks during the 2015 Arctic Sea State research cruise. The depth profiles of water isotopes, salinity, and ice texture for these sea ice cores were examined to provide information about the development of refrozen melt ponds and water balance generation processes, which are otherwise difficult to acquire. The presence of meteoric water with low oxygen isotope values as relatively thin layers indicates melt pond water stability and little mixing during formation and refreezing. The hydrochemical characteristics of refrozen melt pond and seawater depth profiles indicate little snowmelt enters the upper ocean during melt pond refreezing. Due to the seasonal characters of deuterium excess for Arctic precipitation, water balance calculations utilizing two isotopic tracers (oxygen isotope and deuterium excess) suggest that besides the melt of snow cover, the precipitation input in the melt season may also play a role in the evolution of melt ponds. The dual-isotope mixing model developed here may become more valuable in a future scenario of increasing Arctic precipitation. The layers of meteoric origin were found at different depths in the refrozen melt pond ice cores. Surface topography information collected at several core sites was examined for possible explanations of different structures of refrozen melt ponds.

Plain Language Summary The connection between precipitation and the retreat and expansion of sea ice is poorly understood. This paper brings a new approach to investigate meteoric origins of sea ice in the polar regions. We propose to investigate moisture sources for precipitations and the accumulation of snow based on isotopic analysis of sea ice samples from the Arctic. Better understanding of the moisture sources of precipitation in the polar regions will help us constrain models and predictions of glacial and sea ice coverage of the polar regions under current and future climate conditions. In this paper, depth profiles of stable isotopes, salinity, and ice texture of sea ice samples were described to serve as illustrations of the structures of the refrozen melt ponds in the Arctic. An isotope tracer mixing model was developed to determine the seasonality of meteoric water input for sea ice water balance.

Key Points:
- The presence of meteoric origin isotopic signals as relatively thin layers indicates melt pond water stability during refreezing
- A dual-isotope (oxygen isotope and deuterium excess) mixing model was utilized to determine the seasonality of meteoric water input
- The meteoric water signals of refrozen melt ponds were found near the surface or bottom, which may be due to different surface topography

Supporting Information:
- Supporting Information S1
- Data Set S1
- Data Set S2
- Data Set S3

Correspondence to:
Y. Gao,
yongli.gao@utsa.edu

Citation:
Tian, L., Gao, Y., Ackley, S. F., Stammerjohn, S., Maksym, T., & Weissling, B. (2018). Stable isotope clues to the formation and evolution of refrozen melt ponds on Arctic sea ice. *Journal of Geophysical Research: Oceans*, *123*, 8887–8901. https://doi.org/10.1029/2018JC013797

Received 13 JAN 2018
Accepted 7 NOV 2018
Accepted article online 15 NOV 2018
Published online 7 DEC 2018

1. Introduction

Observational data of the average temperature of the Earth's climate system have shown an unequivocal pattern of planetary warming (Intergovernmental Panel on Climate Change, 2014). The Arctic is warming twice as fast as the global average because of a well-documented effect known as Arctic amplification of global warming (Bekryaev et al., 2010; Serreze & Francis, 2006). Both satellite observations and field measurements indicated the overall trend of the shrinking sea ice extent (e.g., Parkinson & DiGirolamo, 2016), decreasing sea ice thickness and volume (e.g., Laxon et al., 2013), and profound loss of multiyear sea ice (e.g., Tschudi et al., 2016) in the Arctic over the past few decades. The diminishing sea ice has had a leading role in recent Arctic temperature amplification through positive ice-albedo feedback (Screen & Simmonds, 2010) by moderating the heat exchange between the ocean and atmosphere. Sea ice also interacts with the broader climate system via oceanic feedback involving sea ice growth/melt and the freshwater balance at the ocean surface (Lewis et al., 2012).

Despite the fundamental importance of sea ice changes for global climate change, there are numerous gaps in our understanding of sea ice system function in the atmosphere-ice-ocean thermodynamic processes and the causes of the observed sea ice reduction in the Arctic. In particular, information is limited regarding the

mechanisms of sea ice melt pond formation and evolution (Flocco et al., 2015). Melt ponds form on Arctic sea ice from the accumulation in topographic depressions of the melting of snow and upper layers of sea ice during the summertime. The presence of melt ponds on the surface of Arctic sea ice plays a critical role in the mass balance of Arctic sea ice through a positive albedo feedback leading to sea ice thinning (Perovich et al., 2007). Previous studies of melt ponds have focused on their spatial distribution (e.g., Fetterer & Untersteiner, 1998; Huang et al., 2016; Rösel & Kaleschke, 2012) and summertime evolution (e.g., Lüthje et al., 2006; Markus et al., 2009; Webster et al., 2015). However, it is still unclear of the hydrochemical characteristics of refrozen melt ponds and whether or not snowmelt enters the upper ocean during melt pond refreezing.

The measurements of stable oxygen and hydrogen isotopes ($\delta^{18}O$ and δD) of water molecules prove to be a useful method in water-related studies because of a robust physically based understanding of isotopic partitioning in the water cycle and hydrologic processes (Araguás-Araguás et al., 2000). Water isotope data are particularly effective for characterizing hydrology and hydroclimatology in remote regions. The $\delta^{18}O$ in sea ice cores has been widely used as a tracer of meteoric water input (e.g., Eicken et al., 2005; Granskog et al., 2017) that may be difficult or impossible to acquire using other methods. The water isotope parameter deuterium excess (d), which is an indicator of moisture source conditions, can also serve as a tracer to help understand hydrological changes due to sea ice loss (Klein & Welker, 2016). Kopec et al. (2016) used the precipitation d to determine changes in the proportion of moisture sourced from the Arctic with sea ice change over the past two decades. However, there are no reports on the application of deuterium excess in sea ice cores to determine the seasonality of meteoric water signals in isotopic depth profiles.

Analyses of nine cores taken from multiyear sea ice refrozen melt ponds and adjacent hummocks during the October 2015 Arctic Sea State research cruise (see Thomson et al., 2018, for the cruise overview) are presented to provide information on the development of refrozen melt ponds and water balance generation processes. A total of 84 sea ice samples, together with 5 snow samples and 5 seawater samples collected during the cruise for stable isotope analyses, is presented in this paper. Depth profiles of stable isotopes, salinity, and ice texture for the nine cores were described to serve as an illustration of structures of refrozen melt ponds. In contrast to previous studies that used only $\delta^{18}O$ tracer to calculate the meteoric water fraction in sea ice cores, we applied an updated two isotopic tracer ($\delta^{18}O$ and d) mixing model in our water balance calculations. To our knowledge, this is the first attempt on this application to examine seasonality of meteoric water input in refrozen melt ponds in the Arctic. Surface topography information collected at several core sites was examined for possible explanations of the different structures of the refrozen melt ponds.

2. Materials and Methods

2.1. Sampling and Field Measurements

Sea ice cores were collected during the Arctic Sea State research cruise on research vessel Sikuliaq in the Beaufort and Chukchi Seas from 28 September to 10 November 2015 (Figure 1a). The main goal of this research cruise was to observe the fall ice advance and the interactions with winds and waves. A remnant tongue of ice persisted in the Beaufort Sea throughout much of summer 2015, which created a region of cooler sea surface temperature in autumn 2015 (Figure 1a). During this 6-week research cruise, the ice edge moved 250 nautical miles (463 km) southward from the summer ice minimum in the Beaufort and Chukchi Seas, reaching the Alaskan coast (Thomson et al., 2017). The program also observed many multiyear sea ice floes with nine cores drilled on refrozen melt ponds and adjacent hummocks at two different multiyear ice floes: Ice Station 1 (IS #1, Figure 1b) and Ice Station 5 (IS #5, Figure 1c). The IS #1 is the furthest north point of the cruise with a larger size than the IS #5 (Figure 1).

On IS #1, three sea ice cores were drilled in depressed areas and one core in an adjacent hummock. On IS #5, four sea ice cores were drilled in the depressed areas and one core in an adjacent hummock. We carried out snow depth surveys for both ice stations using a GPS snow depth probe (Snow-Hydro® MagnaProbe), which has an accuracy of 0.3 cm on level sea ice and snow. A LiDAR survey was conducted in a 100-m × 100-m section on IS #1, and the four ice cores collected on IS #1 were within this section. Comparison of the structures of refrozen melt ponds between the two ice floes and cores with different surface relief could demonstrate the effect of surface topography on the melt pond formation and evolution. Sampling

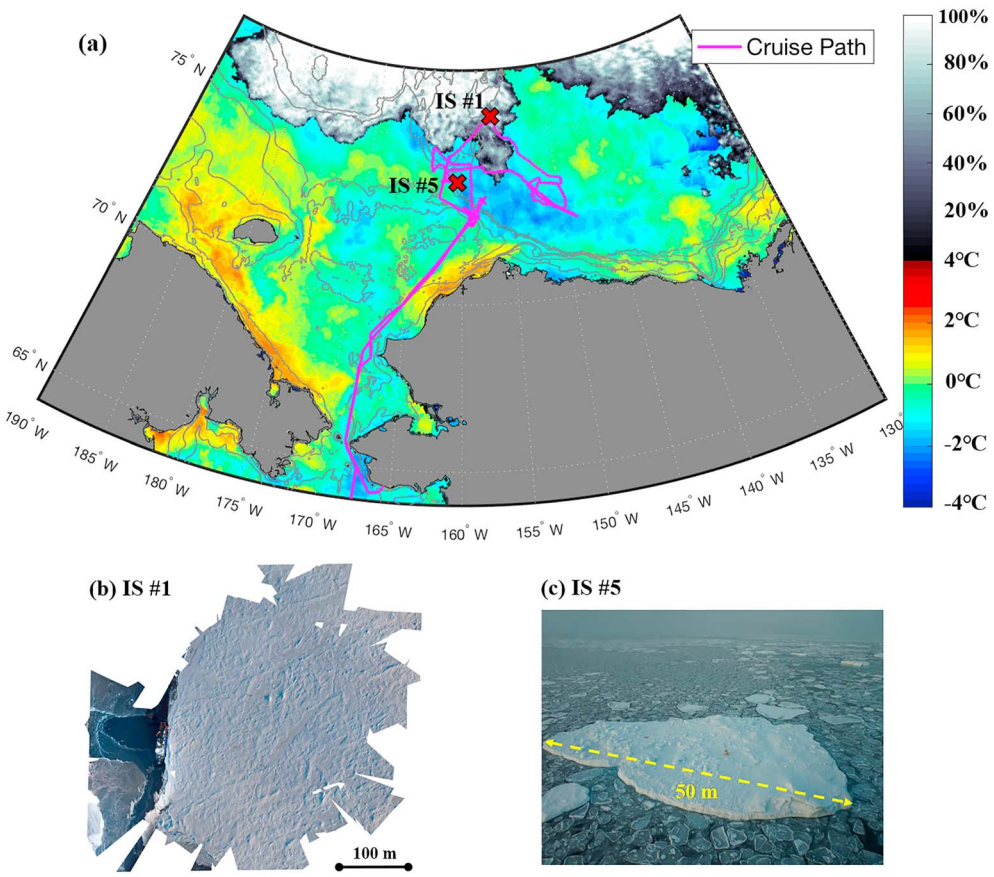

Figure 1. Sikuliaq 2015 Arctic Sea State research cruise track with locations of ice stations (a) and aerial photo mosaic of Ice Station 1 (b) and a photo of Ice Station 5 from the ship's bridge (c). Base map adopted from Thomson et al. (2018), which shows the sea surface temperature anomaly (colors, derived from sea surface temperature data available at https://mur.jpl.nasa.gov) and ice cover (gray scale, derived from AMSR2, data available at https://seaice.uni-bremen.de) in the western Arctic on 1 October 2015.

information, core description, and surface topography for the nine cores collected for water isotope analysis are given in Table 1.

The cores were placed in plastic bags and transferred to a cold room (−20 °C) onboard the R/V Sikuliaq. Each core was cut in half vertically using a bandsaw and a vertical thick section slice taken from the center of one half. The half core was then cut into 10-cm vertical sections, and 1/4 of each core section was melted in a separate container. Salinity was measured with a conductivity probe and meter (Beckman Coulter®) for each melted subsample. The salinity aliquots were decanted into glass bottles, capped with no headspace, sealed with parafilm, and stored in a refrigerator for future water isotope analyses. The ice texture of each section was examined using the thick sections placed between crossed polaroids on a light table onboard (Weeks & Ackley, 1986).

Besides the stable isotope analyses of sea ice samples, snow and seawater samples were also collected during the cruise for reference of the endmembers for isotopic values of meteoric water and seawater. Five snow samples from different ice stations were collected, melted, and stored in sealed bottles. A ship's conductivity-temperature-depth cast was conducted near IS #1 with measurements of salinity and five seawater samples from the surface to 200-m depth were also collected for stable isotope analysis (Table 1).

2.2. Analysis of Water Isotope Ratios

A total of 94 sea ice, snow, and seawater samples was collected for stable isotope analysis. The $\delta^{18}O$ and δD measurements of these samples were performed on a Picarro L2130-i water isotope analyzer (cavity

Table 1
Summary of Sea Ice Cores and Seawater Profile With Sampling Information, Core Information, Surface Topography, Snow Depth, and Bulk Salinity

Ice station	Date	Location	Core no.	Core depth	Sample size	Surface topography	Snow depth (cm)	Bulk salinity (psu)
IS #1	8 October 2015	75.307°N	1.1	40 cm	6	Depressed area	4	1.4
		156.170°W	1.2	32 cm	6	Depressed area	3	1.0
			1.3	34 cm	7	Depressed area	3	0.7
			1.4	158 cm	24	Hummock	0.3	1.1
			NA	200 m	5	Seawater	NA	30.4
IS #5	18 October 2015	73.795°N	5.1	64 cm	10	Depressed area	6	1.2
		160.299°W	5.2	23 cm[a]	5	Depressed area	4.5	3.7
			5.3	65 cm	10	Depressed area	4.3	1.9
			5.4	70 cm	10	Depressed area	4.1	2.1
			5.5	43 cm[a]	6	Hummock	0.3	0.6

Note. NA = not available.
[a]These cores are partial cores due to time limitations on the sampling.

ring-down spectroscopy, CRDS) in the Department of Geological Sciences, University of Texas at San Antonio. Results are reported as relative to the standard Vienna Standard Mean Ocean Water (VSMOW). The measurement precisions for $\delta^{18}O$ and δD were 0.1‰ and 0.4‰, respectively. The $\delta^{18}O$ and δD are given in the following equations:

$$\delta^{18}O = \left[\left({}^{18}O/{}^{16}O\right)_{Sample} - \left({}^{18}O/{}^{16}O\right)_{VSMOW}\right] / \left({}^{18}O/{}^{16}O\right)_{VSMOW} \times 10^3 \quad ‰ \tag{1}$$

$$\delta D = \left[(D/H)_{Sample} - (D/H)_{VSMOW}\right] / (D/H)_{VSMOW} \times 10^3 \quad ‰ \tag{2}$$

Deuterium excess (d), a second-order parameter, which combines both oxygen and hydrogen isotopic species, is defined by the following expression (Dansgaard, 1964). Standard deviations for deuterium excess measurements were lower than 0.5‰ base on analyses of $\delta^{18}O$ and δD for random duplicate samples and calculation of d using following equation.

$$d = \delta D - 8 \times \delta^{18}O \quad ‰ \tag{3}$$

Most previous sea ice isotopic results have been measured using traditional isotope ratio mass spectrometry instruments. The CRDS-based $\delta^{18}O$ measurements of both freshwater (Benetti et al., 2016) and seawater (Walker et al., 2016) have been found to be equivalent to high-quality measurements by isotope ratio mass spectrometry. The salt effect (Benetti et al., 2017) on $\delta^{18}O$ and δD measurement of seawater is within the range for CRDS analytical uncertainty if the vaporizer is frequently cleaned (Skrzypek & Ford, 2014). The salt effect is negligible for our multiyear sea ice and snow samples due to their low salinity (<7 psu). The CRDS technology could measure the $\delta^{18}O$ and δD simultaneously, to calculate the d using equation (3). Although many recent sea ice isotopic studies have utilized the CRDS technology (e.g., Geilfus et al., 2015; Granskog et al., 2017), there is no report about the application of deuterium excess in sea ice water balance generation processes in these studies.

2.3. Stable Isotope Mixing Model

Both $\delta^{18}O$ and salinity were usually utilized as tracers to solve the freshwater budget for seawater mass balance in polar oceans (e.g., Meredith et al., 2017, 2013; Östlund & Hut, 1984). Some early sea ice mass balance studies also used both $\delta^{18}O$ and salinity as tracers (e.g., Jeffries et al., 1989; Lange et al., 1990). However, sea ice is not a closed system for salinity due to brine rejection and gravity drainage processes (Weeks & Ackley, 1986). Most previous investigations have only used $\delta^{18}O$ as an index tracer to calculate the percentages of core length that contains meteoric water (e.g., Eicken et al., 2005) or derive meteoric water fraction in sea ice cores (e.g., Granskog et al., 2017). This one-tracer for two-component model can be utilized to calculate the meteoric water fraction in sea ice cores based on the following equation:

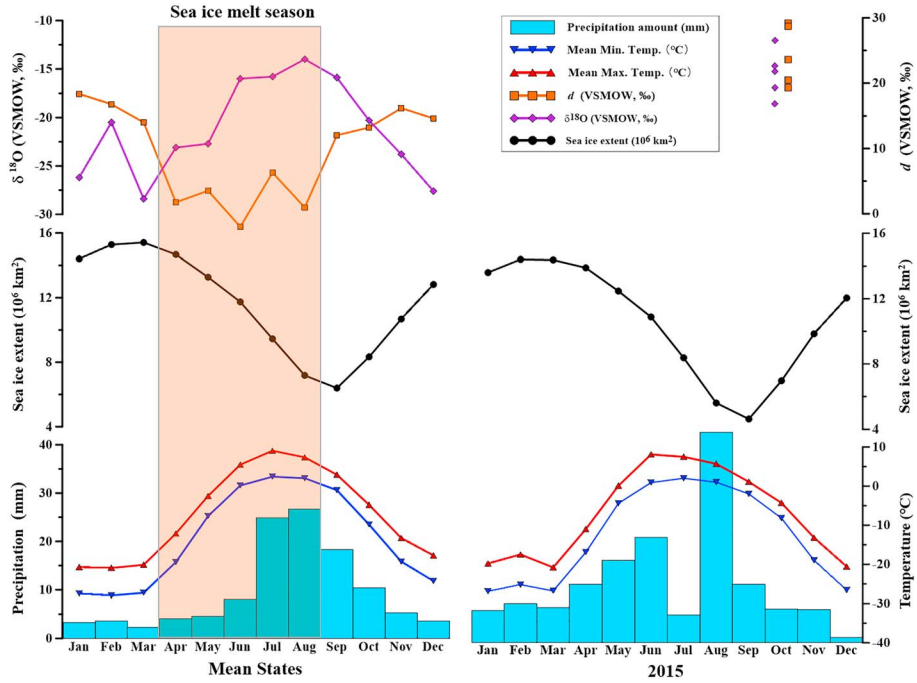

Figure 2. (top panel) Modeled monthly precipitation $\delta^{18}O$ and deuterium excess in Barrow, Alaska, for the long-term means of 1950 to present (left), which were calculated using the Online Isotopes in Precipitation Calculator (http://www.waterisotopes.org). The $\delta^{18}O$ and *d* of snow samples collected during the Sikuliaq October 2015 cruise (right). (middle panel) Monthly sea ice extent for long-term means of 1981–2010 (left) and 2015 (right). Data are available at the National Snow and Ice Data Center (http://www.nsidc.org/data/seaice). (bottom panel) Monthly precipitation amount, maximum temperature, and minimum temperature for long-term means of 1981–2010 (left) and 2015 (right) at a meteorological station in Barrow, Alaska. Data are available at the National Climatic Data Center (http://www.ncdc.noaa.gov). VSMOW = Vienna Standard Mean Ocean Water.

$$\delta^{18}O_S\,(1 - F_M) + \delta^{18}O_M\,F_M = \delta^{18}O_{Sample} \tag{4}$$

where F_M is the unknown fraction of *meteoric water*. The $\delta^{18}O_S$ and $\delta^{18}O_M$ are oxygen isotope values for *seawater* and meteoric water sources, respectively. The endmembers for $\delta^{18}O_S$ and $\delta^{18}O_M$ are assigned later for water balance calculations.

Deuterium excess has been widely used to identify source regions of precipitation (Cui et al., 2009; Lewis et al., 2013; Steen-Larsen et al., 2015), and it also has been successfully applied to ice core records from Tibetan Plateau glaciers (Zhao et al., 2012), Antarctic ice sheet (Stenni et al., 2010), and Greenland ice sheet (Klein & Welker, 2016). Motivated by Kopec et al. (2016), who suggest that precipitation with lower *d* values indicates increasing Arctic-sourced moisture associated with the recent reduction of sea ice, we apply *d* to examine the possible seasonality of meteoric water input in refrozen melt ponds on Arctic sea ice. The seasonality of the meteoric water isotopes is verified using the modeled mean monthly precipitation $\delta^{18}O$ and *d* in Barrow, Alaska, which is the nearest weather station for our sampling sites (Figure 2).

As shown in Figure 2, Arctic sea ice extent usually reaches its maximum in March and minimum in September. The modeled monthly precipitation $\delta^{18}O$ in Barrow show seasonal changes: The monthly precipitation $\delta^{18}O$ have a wide range from −15.9‰ to −28.4‰ during the sea ice growth season (from September to next March) and an overlapping range from −14‰ to −23.1‰ during the sea ice melt season (from April to August). However, our measurements for seawater $\delta^{18}O$ show a relatively narrow range from −1.2‰ to −3.5‰, which is significantly different from meteoric water $\delta^{18}O$. Therefore, $\delta^{18}O$ is a valid tracer to distinguish the meteoric water and seawater contributors.

The *d* of the precipitation in Barrow shows two distinct ranges between the sea ice melt season (from −2 to 6.4‰) and the sea ice growth season (from 12.2‰ to 18.6‰), due to increased locally evaporated Arctic moisture with low *d* in the sea ice melt season and increased moisture from subtropical regions with high

d in the sea ice growth season (Kopec et al., 2016). The *d* of precipitation with distinct values between the sea ice growth season and melt season enables us to distinguish the contributions of meltwater from snow cover and precipitation input in the melt season in sea ice water balance generation processes.

Here we use a two-tracer for three-component model to calculate the mixing ratio based on the following equations:

$$F_S + F_{SM} + F_P = 1 \tag{5}$$

$$\delta^{18}O_S\, F_S + \delta^{18}O_{SM}\, F_{SM} + \delta^{18}O_P\, F_P = \delta^{18}O_{Sample} \tag{6}$$

$$d_S\, F_S + d_{SM}\, F_{SM} + d_P\, F_P = d_{Sample} \tag{7}$$

where F_S, F_{SM}, and F_P are the unknown fractions in the assumed three-component mixture of seawater, *snowmelt* (meltwater from snow cover, i.e., precipitation in the sea ice growth season), and *precipitation input* (precipitation falling on the melt ponds, i.e., precipitation in the sea ice melt season), respectively, during the water balance generation processes. The $\delta^{18}O_S$, $\delta^{18}O_{SM}$, and $\delta^{18}O_P$ are oxygen isotope values, while d_S, d_{SM}, and d_P are deuterium excess values of these components. The endmembers for $\delta^{18}O$ and *d* are assigned later for water balance calculations.

3. Results and Discussion

3.1. Water Isotopes, Salinity, and Texture Profiles

The depth profiles of water isotopes, salinity, and ice texture of nine sea ice cores and one seawater profile at IS #1 are shown in Figure 3 and listed in supporting information Table S1.

As shown in Figure 3 and supporting information Table S1, the $\delta^{18}O$ values for all sea ice cores vary from −0.5‰ to −17.2‰, while the $\delta^{18}O$ values for the seawater increase from −3.5‰ at the surface to −1.2‰ at 200-m depth. For IS #1, Cores 1.2 and 1.3 from depressed areas both showed the low $\delta^{18}O$ signals at depths between 5 and 10 cm; Core 1.1 from depressed areas appeared with low $\delta^{18}O$ signal at a greater depth (40 cm); and the Core 1.4 from a hummock also showed a low signal at greater depth (80 cm). For IS #5, Cores 5.1, 5.2, and 5.3, all taken from more depressed areas, showed low $\delta^{18}O$ signals at depths between 3 and 25 cm; Core 5.4 from a depressed area with a slightly low $\delta^{18}O$ signal at the 10- to 16-cm section; and Core 5.5 from a hummock has generally higher $\delta^{18}O$ signal with no particular pattern.

The refrozen meteoric water layers with low $\delta^{18}O$ values normally were detected in the upper-middle portion of the cores covered by surface ice lid with relatively high $\delta^{18}O$ values. Only Core 1.1 occurs with refrozen meteoric water near the bottom. Meteoric water layers appeared in all the sea ice cores except Core 5.5 (a hummock core) indicates that limited amount of snowmelt entered the upper ocean during melt pond refreezing. The presence of meteoric water with low $\delta^{18}O$ signals as relatively thin layers indicates melt pond water stability and little mixing during melt pond refreezing, which is not captured by the present melt pond models and simulations (Flocco et al., 2015) where mixing and overturning are proposed in the melt pond refreezing process.

As shown in Figure 3 and supporting information Table S1, the *d* values for all sea ice cores vary from −0.5‰ to −8.6‰, while the *d* values for the seawater profile vary from 0.7‰ to 1.5‰. Overall, *d* is less variable than $\delta^{18}O$ in all the profiles. And *d* profiles show clear negatively correlated relationships with $\delta^{18}O$ profiles in refrozen melt pond cores at IS #1: the lowest $\delta^{18}O$ corresponding to the highest *d* in the same section, which indicate that the meteoric water layers in these cores are mainly contributed from snowmelt; all the other meteoric water layers with low $\delta^{18}O$ signals corresponding to relatively low *d* signal might have higher percentages of precipitation input, which are verified by water balance calculations later. The lack of high *d* signal in the upper ocean confirmed that little snowmelt was present in the upper ocean at the time of sampling.

The bulk salinity of all the sea ice cores varies between 0.6 and 3.7 psu, while in the seawater profile at IS #1, the salinity increases from 26 psu at the surface to 32 psu at 200-m depth (Table 1 and Figure 3). The salinity of our sea ice samples, from both refrozen melt pond and hummock cores, is generally lower than those previously reported in Weeks and Ackley (1986) for multiyear sea ice. Subjective observations (made by S. F. Ackley and S. Stammerjohn) during coring of these ice samples indicated that they were generally

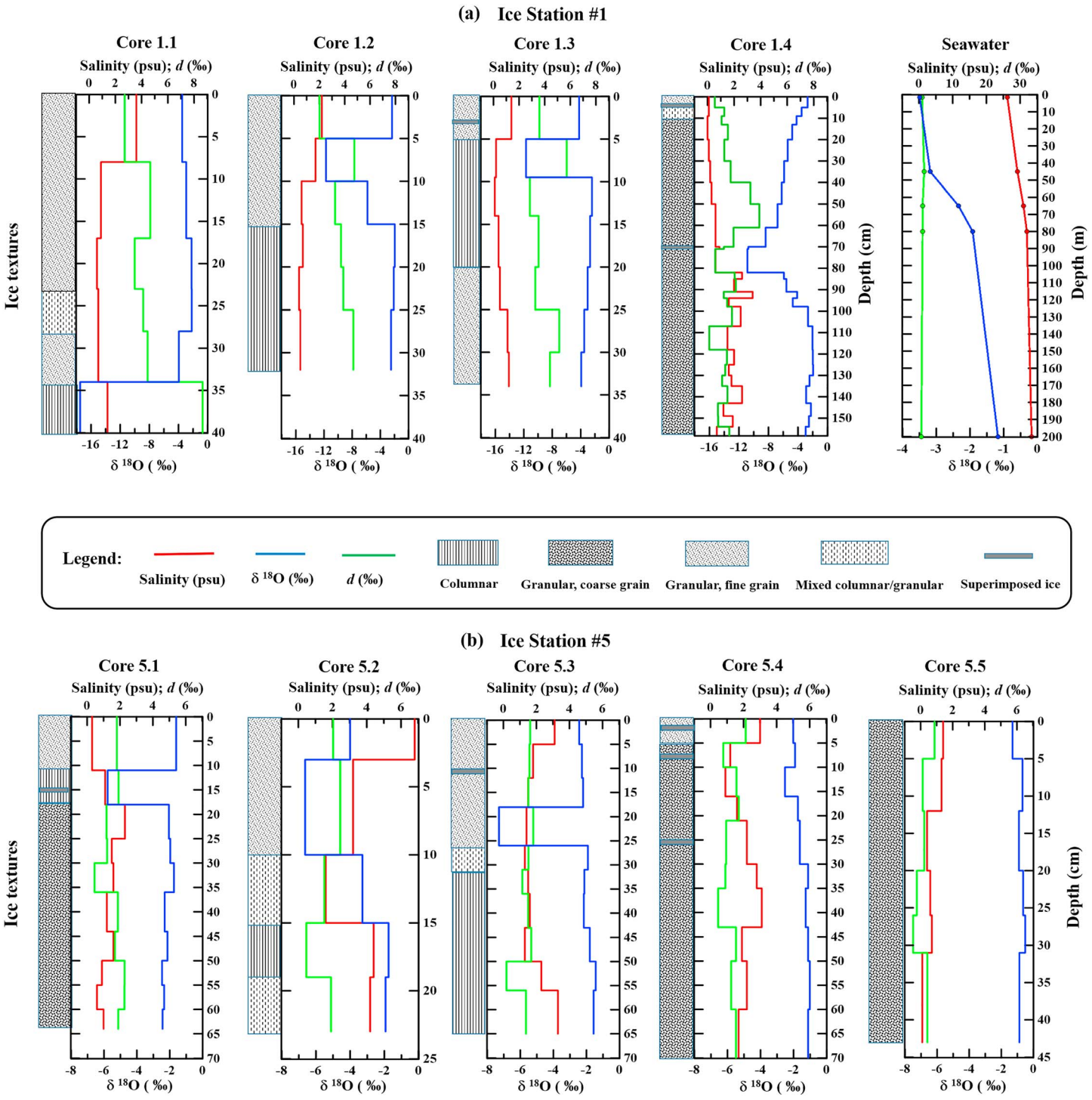

Figure 3. Ice texture, salinity, and water isotope profiles for nine sea ice cores collected on Ice Station 1 (a) and Ice Station 5 (b). The seawater salinity and water isotope profiles near IS #1 were also shown in (a).

more brittle than normal sea ice and more similar to freshwater ice, which is consistent with their low salinity as well as their coarse granular texture, which can also develop in freshwater bodies. The thickness-weighted mean bulk salinity for IS #1 (1.1 psu) and IS #5 (1.7 psu) are significantly lower than the recently reported bulk salinity for second-year sea ice (2.7 psu) and first-year sea ice (4.9 psu) north of Svalbard (Granskog et al., 2017), which indicated that the two multiyear ice floes might have experienced more than one previous

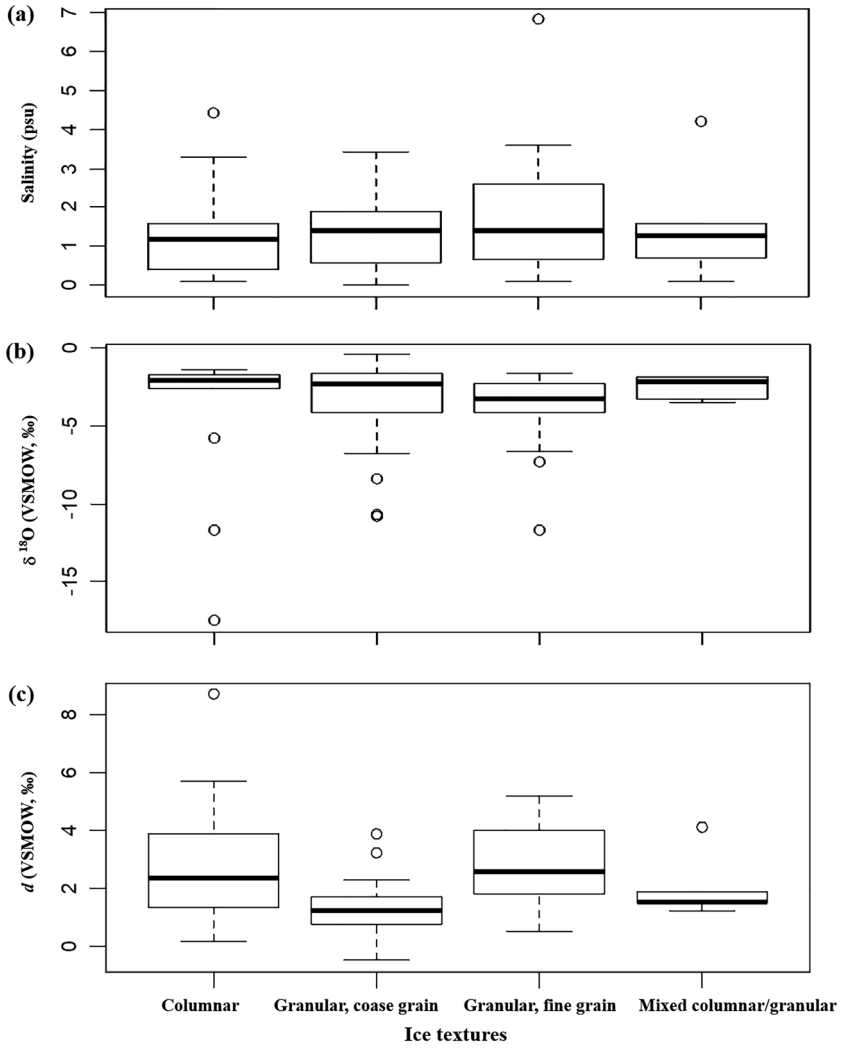

Figure 4. Boxplot for salinity (a), $\delta^{18}O$ (b), and deuterium excess (c) among the four classes of ice textures. VSMOW = Vienna Standard Mean Ocean Water.

melt-freezing cycle. The salinity was not correlated with $\delta^{18}O$ in all ice core profiles, which indicated the desalination has less impact on the $\delta^{18}O$ signal.

There are four classes of ice textures: columnar (n = 14), granular with coarse grain (n = 45), granular with fine grain (n = 20), and mixture of columnar/granular (n = 5). The nine cores show variable contributions of granular ice from 40% to 100% of the total length of these cores (Figure 3 and supporting information Table S1), significantly higher than the observations from earlier studies in the Arctic basin (Eicken et al., 1995; Granskog et al., 2017; Perovich et al., 2009). The high granular ice contribution in these ice cores is different from typical columnar refrozen melt pond structure; however, the causes are still unknown. There are no typical surface granular layers with low $\delta^{18}O$ signals (cf. Granskog et al., 2017) found in our ice cores, which indicated that the snowmelt percolated down the ice column. Only thin layers of ice (a few millimeters thick) of superimposed ice, formed by the refreezing of snow meltwater on the colder ice, were detected in several sections (Figure 3). However, this type of ice made up a small portion of these ice sections ($<$5%) and a negligible portion of the whole cores. Thus, the $\delta^{18}O$ signature of any superimposed ice may be diluted due to the sampling. These superimposed ice layers in several cores may have survived the surface melt during a previous summer, which would also support the suggestion that these two sea ice floes are second year ice or older, as indicated by the low salinity and hummocky surface. Ice textures are also examined with their relationship with salinity and water isotope signals. The boxplot for salinity (Figure 4a), $\delta^{18}O$ (Figure 4b),

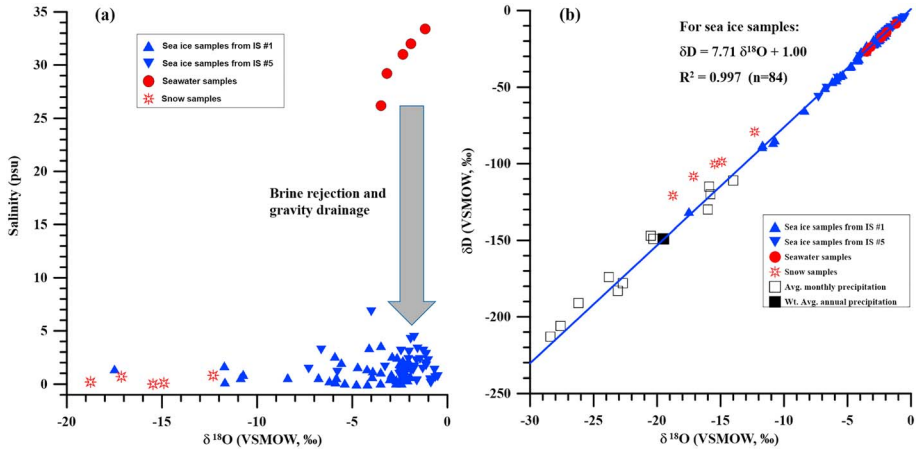

Figure 5. Cross plot of $\delta^{18}O$ against salinity (a) and $\delta^{18}O$ against δD (b) for the sea ice, snow, seawater samples, which were collected during Sikuliaq October 2015 research cruise and modeled monthly/annual precipitation isotopes in Barrow, Alaska, calculated using the Online Isotopes in Precipitation Calculator (http://www.waterisotopes.org). VSMOW = Vienna Standard Mean Ocean Water.

and deuterium excess (Figure 4c) of the four classes suggest little difference for mean isotopic and salinity values among different ice textures. However, no firm conclusions were drawn by the limited amount of data.

3.2. Water Balance Calculations

As shown in Figure 5a, the salinity is not suitable as a tracer because of brine rejection during the sea ice formation and gravity drainage during sea ice melt; that is, the ice core is not a closed system for salinity. Some other studies have used the relationship of $\delta^{18}O$ and salinity to determine the evapoconcentration effect (Phillips et al., 2003; Yuan et al., 2011) because evaporation enriches water bodies with heavy isotopes and also elevates salinity. Our sea ice sample data do not show a positive correlation between salinity and $\delta^{18}O$. We conclude that the sea ice isotope signal is mainly controlled by a mixing process of meteoric water and seawater without an evapoconcentration effect.

As shown in Figure 5b, $\delta^{18}O$ against δD for all the sea ice samples show a significant linear relationship: $\delta D = 7.71 \times \delta^{18}O + 1.00$ ($N = 84$; $R^2 = 0.997$). All sea ice samples align on a straight line with a slope very close to the Global Meteoric Water Line $\delta D = 8 \times \delta^{18}O + 10$ (Craig, 1961). The d change is considered negligible between sea ice and its parent water during the freezing process because the freezing slope is near 8 (Souchez et al., 2000). Although the snow samples with high d are slightly above the trendline of the sea ice samples, all the monthly precipitation and seawater samples fall on the trendline, which indicates that the signal of meteoric water and seawater d would be conservative in the freezing and mixing process of meteoric water and seawater.

The water balance calculation utilizes the IsoError dual-isotope three-source model described by Phillips and Gregg (2001). This mixing model calculates estimates and confidence intervals of source proportional contributions to a mixture using stable isotope analyses. For dual-isotope studies, the measurements of the two isotope signatures for samples from the mixture population and three-source populations should be independent of each other (Phillips & Gregg, 2001). While there is a significant linear relationship between $\delta^{18}O$ and δD among sea ice samples, seawater samples, and monthly precipitation (Figure 5b), no significant correlation was observed between d and $\delta^{18}O$ among the mixture and the three sources (Figure 6); that is, the $\delta^{18}O$ and δD are dependent on each other, and $\delta^{18}O$ and d are independent variables.

As shown in Figure 6, there are overlapping ranges of $\delta^{18}O$ for the monthly precipitation during the sea ice melt season and sea ice growth season. However, the precipitation d in the sea ice melt season is much lower than the precipitation d during the sea ice growth season. The mean isotopic values for each ice core are within the mixing lines between the three endmembers of seawater, snowmelt, and precipitation input. However, there are many ice sections from IS#1 with isotopic values outside from the main triangle but falling on the mixing line between seawater and snow samples. Therefore, we could derive three source proportions

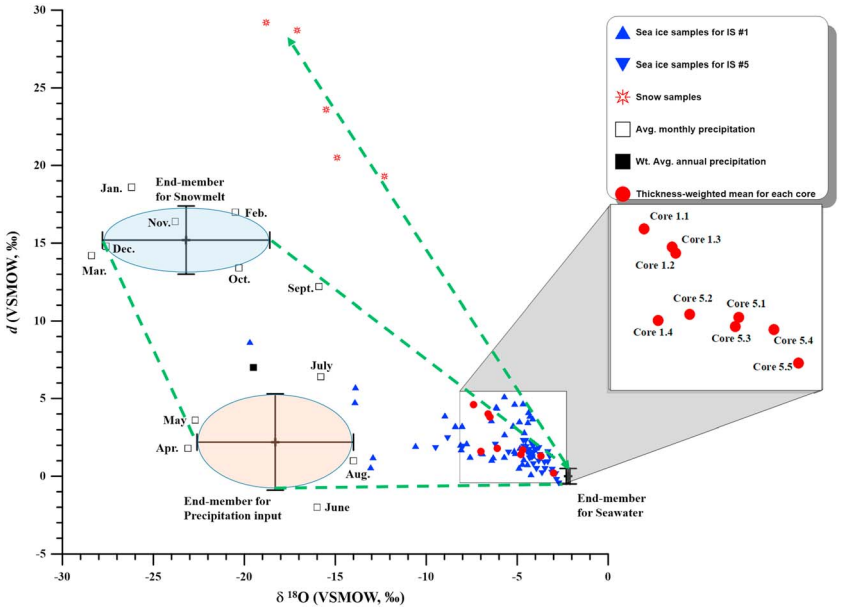

Figure 6. Partitioning contributions of *seawater*, *snowmelt*, and *precipitation input* for all sea ice cores and sea ice sections using dual-isotope ($\delta^{18}O$ and deuterium excess) mixing model. The green dashed lines are the mixing lines between these three endmembers and possible mixing line between seawater and snow samples. Please note that $\delta^{18}O$ values for all ice cores and ice sections have adjusted with negative shift 2.2‰. VSMOW = Vienna Standard Mean Ocean Water.

using the dual-isotope mixing model for all ice cores (Table 2) but not for all ice sections (supporting information Table S3).

The three endmembers of seawater, snowmelt, and precipitation input for this dual-isotope mixing model were provided with the mean ± standard deviation (Figure 6). Modeled long-term mean annual and monthly precipitation $\delta^{18}O$ and *d* in Barrow are listed in supporting information Table S2. The mean with one standard deviation of $\delta^{18}O$ for precipitation in the sea ice growth season (September–March) and precipitation in the sea ice melt season (April–July) are −23.2 ± 4.6‰ (n = 7) and −18.3 ± 4.3‰ (n = 5), respectively. Therefore, the corresponding values of the $\delta^{18}O$ endmembers for snowmelt and precipitation input are $\delta^{18}O_{SM}$ = −23.2 ± 4.6‰ and $\delta^{18}O_P$ = −18.3 ± 4.3‰. We also directly use the mean with one standard deviation of *d* for our sea ice growth season precipitation and sea ice melt season precipitation as our *d* endmembers: d_{SM} = 15.2 ± 2.2‰, d_P = 2.2 ± 3.1‰.

Previously derived effective fractionation coefficients for Arctic sea ice $\delta^{18}O$ near Barrow have a range from 1.8‰ to 2.5‰ (Smith et al., 2016), which indicates sea ice have a mean positive shift of about 2.2‰ from

Table 2
Summary of Sea Ice Cores With the Mean and Range of $\delta^{18}O$ and d and Thickness Percentages of Three Source Proportions: F_S (Seawater Fraction), F_{SM} (Snowmelt Fraction), and F_P (Precipitation Input Fraction)

Ice station	Core no.	$\delta^{18}O$ range (‰)	Mean $\delta^{18}O$ (‰)	*d* range (‰)	Mean *d* (‰)	F_S (%)	F_{SM} (%)	F_P (%)	F_M (%)
IS #1	1	(−17.5, −2.2)	−5.2	(2.7, 8.6)	4.6	68–86	25–38	0–2	30
	2	(−11.7, −2.0)	−4.3	(2.0, 4.8)	3.8	74–88	21–32	0–2	25
	3	(−11.7, −2.4)	−4.4	(2.8, 5.7)	4.0	73–89	22–33	0–1	25
	4	(−10.9, −2.0)	−4.8	(0.1, 3.9)	1.6	66–79	1–14	10–30	28
IS #5	1	(−5.8, −1.6)	−2.5	(0.4, 2.3)	1.7	85–91	7–15	0–7	14
	2	(−6.6, −1.7)	−3.9	(0.5, 2.5)	1.8	75–83	5–15	4–18	23
	3	(−7.3, −1.4)	−2.6	(0.2, 1.8)	1.4	84–89	4–13	0–11	15
	4	(−2.5, −1.0)	−1.5	(0.5, 2.1)	1.3	91–96	5–13	0–4	9
	5	(−1.3, −0.5)	−0.8	(−0.5, 0.9)	0.2	93–97	0–5	0–10	5

Note. The 95% confidence intervals for the thickness percentages are presented here calculated by the IsoError dual-isotope three-source model (https://www.epa.gov/eco-research/stable-isotope-mixing-models-estimating-source-proportions). Thickness percentage of F_M (meteoric water fraction) for each ice core calculated from the $\delta^{18}O$ mixing model was also shown in the table.

its parent water (mainly seawater) due to freezing fractionation. Our isotopic measurement for the surface seawater sample (at depth of 1.5 m) is $\delta^{18}O = -3.5‰$, $d = 0.95‰$. However, the Arctic seawater isotopic values show strong seasonal variations due to varied contributions of freshwater input, which include river runoff, meteoric water, and ice melt (Eicken et al., 2005; Macdonald et al., 1995; Östlund & Hut, 1984). Among our sea ice samples, the most enriched isotopic values are close to $\delta^{18}O = 0‰$, $d = 0‰$, which could be considered as pure seawater origin signals. Considering that mean freezing fractionation of 2.2% for $\delta^{18}O$ and the d is conservative in the freezing process, the corresponding values chosen for the mixing endmembers (with one measurement standard deviation) of seawater are $\delta^{18}O_S = -2.2 \pm 0.1‰$ and $d_S = 0 \pm 0.5‰$.

Using the $\delta^{18}O$ as the only isotopic tracer, we could calculate the meteoric water fraction in sea ice cores based on the equation (4). Modeled long-term mean annual precipitation $\delta^{18}O$ in Barrow is $-19.5‰$ (supporting information Table S2). The corresponding value of $\delta^{18}O$ for meteoric water component is $\delta^{18}O_M = -19.5‰$. We also use $\delta^{18}O_S = -2.2‰$ for pure seawater component, same as value chosen in the dual-isotope mixing model.

We derived the thickness percentages of three source proportions of F_S (seawater fraction), F_{SM} (snowmelt fraction), and F_P (precipitation input fraction) for the nine cores using the thickness-weighted mean $\delta^{18}O$ and d for each core as $\delta^{18}O_{Sample}$ and d_{Sample}. The $\delta^{18}O_{Sample}$ values for all sea ice cores were adjusted with negative shift 2.2‰ considering the mean effective fractionation coefficients for sea ice $\delta^{18}O$ during freezing (Figure 6). The 95% confidence intervals for the thickness percentages of F_S, F_{SM}, and F_P for each ice core are presented in Table 2. We also derived the thickness percentage of F_M (meteoric water fraction) for each ice core calculated from the $\delta^{18}O$ mixing model (Table 2).

These water balance results indicate that snowmelt-dominated meteoric water signals in refrozen melt pond cores at IS #1 (Cores 1.1, 1.2, and 1.3) are consistent with the characteristic of isotopic profiles for these cores. In contrast, the hummock core at IS #1 (Core 1.4) showed the highest of precipitation input signal but almost no snowmelt signal, which might be due to the buildup of percolation of precipitation in the melt season. Compared with IS #1, the refrozen melt pond cores at IS #5 have an overall higher fraction of precipitation input signals. Possible reasons are that the two ice floes differ in both their location and/or different summer seasons when their melt ponds formed. The meteoric water fraction might include both the snowmelt and precipitation input source proportions. Our derived F_S, F_{SM}, and F_M confirmed this relationship: $F_M \approx F_S + F_{SM}$ (Table 2), which verified the validity of the dual-isotope mixing model.

We also derived the thickness percentages of three source proportions of F_S, F_{SM}, and F_P for each ice section using the dual-isotope mixing model and F_M for each ice section calculated from the $\delta^{18}O$ mixing model (supporting information Table S3). However, the IsoError dual-isotope three-source model returns many contribution estimates <0 for F_P especially at IS #1. The IsoError model utilizes the long-term mean precipitation isotopic values as endmembers, and it works very well for the whole multiyear sea ice cores, which contain layers formed at different seasons. However, for an individual section in these sea ice cores, it might be a mixture of seawater and snowmelt from an individual snow event with isotopic values, which deviates from the endmember of snowmelt (Figure 6). The $\delta^{18}O$ mixing model works better than the dual-isotope model for each individual ice section. However, the endmember values for meteoric water are variable among different sea ice sections. Using the mean annual precipitation $\delta^{18}O$ as a consistent endmember might result in serious bias in the F_M calculation for each individual ice section.

Previous studies demonstrated that snow thickness correlated well with the amount of meteoric water in the ice cores from both the Antarctic (Jeffries et al., 1997) and Arctic (Petrich et al., 2012). In the Antarctic, overall thinner ice cover and higher snow accumulation rates result in the widespread occurrence of surface flooding and snow ice formation (e.g., Jeffries et al., 1994; Maksym & Jeffries, 2001; Maksym & Markus, 2008). However, in the Arctic, it is widely considered that snow depths in relation to ice thickness are rarely high enough to have snow ice formation (Sturm & Massom, 2010). Recent research in the north of Svalbard indicated that there is a trend of increasing snow-to-ice thickness ratio due to thicker snow on thinner sea ice (Rösel et al., 2018), which increased the potential for snow ice formation in the Arctic. While meteoric water fraction (average 19.3%) in the multiyear ice floes of this study is significantly higher than snow fraction in the second-year sea ice (average 14.5%) and first-year sea ice (average 3.9%) north of Svalbard (Granskog

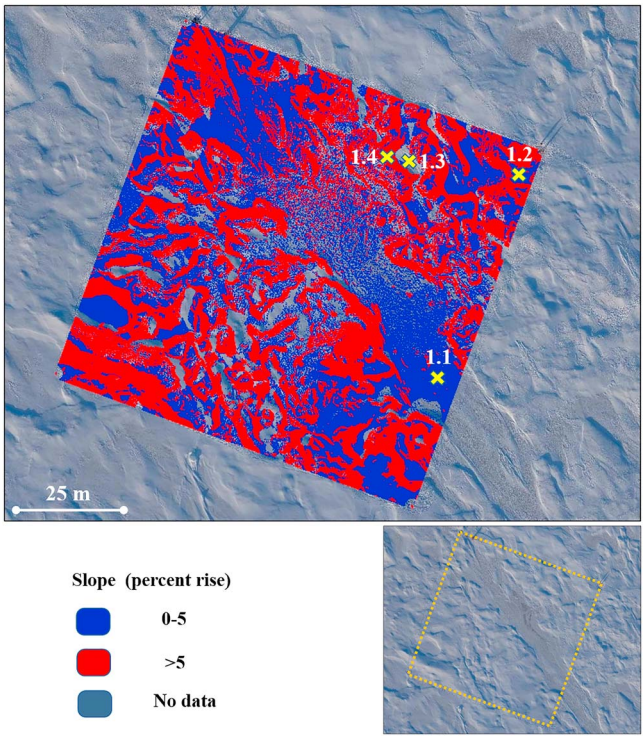

Figure 7. Locations for the four ice cores on Ice Station 1 and LiDAR slope survey results for IS #1. No data areas are the shadow of high areas in the path of the LiDAR beams, that is, also depressed areas with the low surface slope (<5%).

et al., 2017). These differences in meteoric water fraction might be due to sea ice age difference or different sources of meteoric water: snowmelt contribution and drainage into melt ponds in our case and snow ice formation in the ice floes north of Svalbard (Granskog et al., 2017).

We also computed an equivalent depth of snowmelt equivalent (SME):

$$SME = H \times F_{SM} \tag{8}$$

where H is core depth and F_{SM} is the mean thickness percentage of snowmelt fraction here. Using an estimated snow density of 300 kg/m^3 and sea ice density of 900 kg/m^3, the premelt snow depths were estimated as 1-cm SME ~ 3-cm snow, which results in 15.6 to 38.4 cm for the melt pond cores on both ice stations. The premelt snow depths estimated here are consistent with the previously reported mean snow depth of 21 to 34 cm for the Beaufort Sea region (summarized by Sturm & Massom, 2010). However, there are several caveats in using this method as an estimate of the premelt snow depth: The limited sampling of ice cores may not be representative of the mean snow depth; this assumes that no snowmelt enters the upper ocean or is evaporated from the surface; and the melt ponds collect snowmelt from a *catchment area* of unknown dimension (related to the surface topography).

3.3. Effect of Surface Topography on Evolution of Melt Pond

For IS #1, the LiDAR survey results show variations in surface topography with both a large linear melt pond feature as well as a rolling melt pond-hummock topography of 15- to 20-m spacing (Figure 7). As shown in Figure 7, Cores 1.1, 1.2, and 1.3 drilled in the depressed areas with slope $< 5\%$, Core 1.4 drilled in the hummock area with slope $> 5\%$. The refrozen melt pond Core 1.1 is within the linear melt pond with a larger catchment area, while Core 1.2 and Core 1.3 are within isolated round melt ponds with smaller catchment areas. As shown in Figure 3, Core 1.1 appeared with refrozen meltwater at a greater depth (40 cm) than Cores 1.2 and 1.3 (both at 5- to 10-cm depth). For IS #5, all the refrozen melt pond cores are more like isolated round melt ponds with the refrozen meltwater signals in the shallow portions (all at 3 to 25 cm) of the cores.

The sea ice possesses a duality of porosity: isolated melt pond areas with lower permeability, where the intergranular pores in the ice matrix and small fissures dominate (Freitag & Eicken, 2003), and the melt pond with linear features with higher permeability, where fracture and macroscopic flaws such as cracks, leads, enlarged brine channels might exist (Polashenski et al., 2012). Previous research indicates the ice permeability plays a central role in water retention in melt ponds on first year sea ice (Polashenski et al., 2017). Here we use two different conceptual growth models to explain the mechanism controlling the depth of refrozen meteoric water on multiyear sea ice.

Evolution of *isolated round melt ponds* with lower permeability and smaller catchment areas is as follows: (1) Snow cover melt is followed by upper surface sea ice melt during the summer season, which would facilitate smaller and isolated pools at the surface; (2) Drainage happens at the bottom of the melt ponds through the small fissures; (3) Percolation blockage (Polashenski et al., 2017) occurs due to ice accretion within the interior of ice fissures; (4) Ponds refreeze at their upper surface to form an ice lid, until the trapped melt ponds are totally refrozen in the shallow portion of sea ice.

Evolution of *connected linear melt ponds* with higher permeability and larger catchment areas is as follows: (1) Snow cover and sea ice melt during the summer season, which would facilitate significant pooling of snowmelt at the surface; (2) Drainage happens at the bottom of the melt pond through the big fractures; (3) More meltwater and drainage enlarges the fractures and forming conduits, so a large pulse of meltwater would have drained; (4) The meltwater comes into contact with colder seawater, induces the formation of underwater ice (e.g., Eicken et al., 2002), and ultimately becomes a refrozen melt pond at the bottom of the ice column.

These conceptual models are consistent with isotope profiles seen in the depressed areas at both IS #1 and IS #5. However, only Core 1.1 occurs with refrozen meltwater near the bottom. Thus, Core 1.1 could also be somewhat anomalous, which may not be related to its location in a linear melt feature compared to the rounded features of the other melt pond locations. More refrozen ponds cores with differing surface features should be examined in future research.

4. Conclusions

Depth profiles of stable isotopes, salinity, and ice texture were described to serve as illustrations of the structures of the refrozen melt ponds. We utilized a two isotopic tracer (oxygen isotope and deuterium excess) mixing model to determine the seasonality of meteoric water input for sea ice water balance. Surface topography information was examined for possible explanations of different structures of refrozen melt ponds. The main conclusions drawn are as follows:

1. The presence of meteoric water with the low $\delta^{18}O$ signals as relatively thin layers indicates melt pond water stability and little mixing during formation and freezing. This apparent stability differs from the model presented by Flocco et al. (2015). The hydrochemical characteristics of refrozen melt pond and seawater depth profiles indicate little snowmelt enters the upper ocean during melt pond refreezing.
2. Water balance calculations suggest, besides meltwater of snow cover, that the precipitation input in the sea ice melt season also may play an important role in the evolution of melt ponds. The method developed in this paper may become more valuable in a future scenario of increasing Arctic precipitation (Bintanja & Selten, 2014).
3. The meteoric water signals of refrozen melt ponds could be near the surface or deeper in the ice cores, and two growth models—*isolated round melt ponds* and *connected linear melt ponds*—are proposed to explain their possible mechanism. The resulting surface topography shown by a LiDAR survey is consistent with this interpretation, but it is only a working hypothesis because of the small sample size available.

Acknowledgments
The coauthors (S. F. A., S. S., T. M., and B. W.) wish to thank the other DRI participants and the Captain and crew of the Sikuliaq's October 2015 cruise for their assistance in the sample collections analyzed in the paper. Jim Thomson (Chief Scientist), Scott Harper (ONR Program Manager), and Martin Jeffries (ONR Program Manager) are particularly acknowledged for their unwavering assistance and leadership during the 5 years of the SeaState DRI. We thank Guy Williams for production of the aerial photo mosaic. Funding from the Office of Naval Research N00014-13-1-0435 (S. F. A. and B. W.), N00014-13-1-0434 (S. S.), and N00014-13-1-0446 (T. M.) supported this research through grants to UTSA, UColorado, and WHOI, respectively. This project was also funded (in part) by the University of Texas at San Antonio, Office of the Vice President for Research (Y. G. and S. F. A.). Data for the stable isotope mixing models used in this study are shown in supporting information Tables S1–S3.

References

Araguás-Araguás, L., Froehlich, K., & Rozanski, K. (2000). Deuterium and oxygen-18 isotope composition of precipitation and atmospheric moisture. *Hydrological Processes*, *14*(8), 1341–1355. https://doi.org/10.1002/1099-1085(20000615)14:8<1341::AID-HYP983>3.0.CO;2-Z

Bekryaev, R. V., Polyakov, I. V., & Alexeev, V. A. (2010). Role of polar amplification in long-term surface air temperature variations and modern Arctic warming. *Journal of Climate*, *23*(14), 3888–3906. https://doi.org/10.1175/2010JCLI3297.1

Benetti, M., Reverdin, G., Pierre, C., Khatiwala, S., Tournadre, B., Olafsdottir, S., & Naamar, A. (2016). Variability of sea ice melt and meteoric water input in the surface Labrador Current off Newfoundland. *Journal of Geophysical Research: Oceans*, *121*, 2841–2855. https://doi.org/10.1002/2015JC011302

Benetti, M., Sveinbjörnsdóttir, A. E., Ólafsdóttir, R., Leng, M. J., Arrowsmith, C., Debondt, K., et al. (2017). Inter-comparison of salt effect correction for $\delta^{18}O$ and $\delta^{2}H$ measurements in seawater by CRDS and IRMS using the gas-H_2O equilibration method. *Marine Chemistry*, *194*, 114–123. https://doi.org/10.1016/j.marchem.2017.05.010

Bintanja, R., & Selten, F. M. (2014). Future increases in Arctic precipitation linked to local evaporation and sea-ice retreat. *Nature*, *509*(7501), 479–482. https://doi.org/10.1038/nature13259

Craig, H. (1961). Isotopic variations in meteoric waters. *Science*, *133*(3465), 1702–1703. https://doi.org/10.1126/science.133.3465.1702

Cui, J., An, S., Wang, Z., Fang, C., Liu, Y., Yang, H., et al. (2009). Using deuterium excess to determine the sources of high-altitude precipitation: Implications in hydrological relations between sub-alpine forests and alpine meadows. *Journal of Hydrology*, *373*(1–2), 24–33. https://doi.org/10.1016/j.jhydrol.2009.04.005

Dansgaard, W. (1964). Stable isotopes in precipitation. *Tellus*, *16*(4), 436–468. https://doi.org/10.3402/tellusa.v16i4.8993

Eicken, H., Dmitrenko, I., Tyshko, K., Darovskikh, A., Dierking, W., Blahak, U., et al. (2005). Zonation of the Laptev Sea landfast ice cover and its importance in a frozen estuary. *Global and Planetary Change*, *48*(1-3), 55–83. https://doi.org/10.1016/j.gloplacha.2004.12.005

Eicken, H., Krouse, H. R., Kadko, D., & Perovich, D. K. (2002). Tracer studies of pathways and rates of meltwater transport through Arctic summer sea ice. *Journal of Geophysical Research*, *107*(C10), 8046. https://doi.org/10.1029/2000JC000583

Eicken, H., Lensu, M., Leppäranta, M., Tucker, W. B. III, Gow, A. J., & Salmela, O. (1995). Thickness, structure, and properties of level summer multiyear ice in the Eurasian sector of the Arctic Ocean. *Journal of Geophysical Research*, *100*(C11), 22,697–22,710. https://doi.org/10.1029/95JC02188

Fetterer, F., & Untersteiner, N. (1998). Observations of melt ponds on Arctic sea ice. *Journal of Geophysical Research*, *103*(C11), 24,821–24,835. https://doi.org/10.1029/98JC02034

Flocco, D., Feltham, D. L., Bailey, E., & Schroeder, D. (2015). The refreezing of melt ponds on Arctic sea ice. *Journal of Geophysical Research: Oceans*, *120*, 647–659. https://doi.org/10.1002/2014JC010140

Freitag, J., & Eicken, H. (2003). Meltwater circulation and permeability of Arctic summer sea ice derived from hydrological field experiments. *Journal of Glaciology*, *49*(166), 349–358. https://doi.org/10.3189/172756503781830601

Geilfus, N. X., Galley, R. J., Crabeck, O., Papakyriakou, T., Landy, J., Tison, J. L., & Rysgaard, S. (2015). Inorganic carbon dynamics of melt-pond-covered first-year sea ice in the Canadian Arctic. *Biogeosciences*, *12*(6), 2047–2061. https://doi.org/10.5194/bg-12-2047-2015

Granskog, M. A., Rösel, A., Dodd, P. A., Divine, D., Gerland, S., Martma, T., & Leng, M. J. (2017). Snow contribution to first-year and second-year Arctic sea ice mass balance north of Svalbard. *Journal of Geophysical Research: Oceans*, *122*, 2539–2549. https://doi.org/10.1002/2016JC012398

Huang, W., Lu, P., Lei, R., Xie, H., & Li, Z. (2016). Melt pond distribution and geometry in high Arctic sea ice derived from aerial investigations. *Annals of Glaciology*, *57*(73), 105–118. https://doi.org/10.1017/aog.2016.30

Intergovernmental Panel on Climate Change (2014). *Climate change 2013—The physical science basis: Working Group I Contribution to the Fifth Assessment Report of the Intergovernmental Panel on Climate Change*. Cambridge: Cambridge University Press. https://doi.org/10.1017/CBO9781107415324

Jeffries, M. O., Morris, K., Weeks, W. F., & Worby, A. P. (1997). Seasonal variations in the properties and structural composition of sea ice and snow cover in the Bellingshausen and Amundsen Seas, Antarctica. *Journal of Glaciology*, *43*(143), 138–151. https://doi.org/10.3189/S0022143000002902

Jeffries, M. O., Sckinger, W. M., & Serson, H. V. (1989). Stable-isotope ($^{18}O/^{16}O$) tracing of fresh, brackish, and sea ice in multi-year land-fast sea ice, Ellesmere Island, Canada. *Journal of Glaciology*, *35*(119), 9–16. https://doi.org/10.3189/002214389793701473

Jeffries, M. O., Shaw, R. A., Morris, K., Veazey, A. L., & Krouse, H. R. (1994). Crystal structure, stable isotopes ($\delta^{18}O$), and development of sea ice in the Ross, Amundsen, and Bellingshausen seas, Antarctica. *Journal of Geophysical Research*, *99*(C1), 985–995. https://doi.org/10.1029/93JC02057

Klein, E. S., & Welker, J. M. (2016). Influence of sea ice on ocean water vapor isotopes and Greenland ice core records. *Geophysical Research Letters*, *43*, 12,475–12,483. https://doi.org/10.1002/2016GL071748

Kopec, B. G., Feng, X., Michel, F. A., & Posmentier, E. S. (2016). Influence of sea ice on Arctic precipitation. *Proceedings of the National Academy of Sciences*, *113*(1), 46–51. https://doi.org/10.1073/pnas.1504633113

Lange, M., Schlosser, P., Ackley, S., Wadhams, P., & Dieckmann, G. (1990). ^{18}O concentrations in sea ice of the Weddell Sea, Antarctica. *Journal of Glaciology*, *36*(124), 315–323. https://doi.org/10.3189/002214390793701291

Laxon, S. W., Giles, K. A., Ridout, A. L., Wingham, D. J., Willatt, R., Cullen, R., et al. (2013). Cryosat-2 estimates of Arctic sea ice thickness and volume. *Geophysical Research Letters*, *40*, 732–737. https://doi.org/10.1002/grl.50193

Lewis, E. L., Jones, E. P., Lemke, P., Prowse, T. D., & Wadhams, P. (Eds.) (2012). *The freshwater budget of the Arctic Ocean* (Vol. 70). Netherlands: Springer Science & Business Media. https://doi.org/10.1007/978-94-011-4132-1

Lewis, S. C., LeGrande, A. N., Kelley, M., & Schmidt, G. A. (2013). Modeling insights into deuterium excess as an indicator of water vapor source conditions. *Journal of Geophysical Research: Atmospheres*, *118*, 243–262. https://doi.org/10.1029/2012JD017804

Lüthje, M., Feltham, D. L., Taylor, P. D., & Worster, M. G. (2006). Modeling the summertime evolution of sea-ice melt ponds. *Journal of Geophysical Research*, *111*, C02001. https://doi.org/10.1029/2004JC002818

Macdonald, R. W., Paton, D. W., Carmack, E. C., & Omstedt, A. (1995). The freshwater budget and under-ice spreading of Mackenzie River water in the Canadian Beaufort Sea based on salinity and $^{18}O/^{16}O$ measurements in water and ice. *Journal of Geophysical Research*, *100*(C1), 895–919. https://doi.org/10.1029/94JC02700

Maksym, T., & Jeffries, M. O. (2001). Phase and compositional evolution of the flooded layer during snow-ice formation on Antarctic sea ice. *Annals of Glaciology*, *33*, 37–44. https://doi.org/10.3189/172756401781818860

Maksym, T., & Markus, T. (2008). Antarctic sea ice thickness and snow-to-ice conversion from atmospheric reanalysis and passive microwave snow depth. *Journal of Geophysical Research*, *113*, C02S12. https://doi.org/10.1029/2006JC004085

Markus, T., Stroeve, J. C., & Miller, J. (2009). Recent changes in Arctic sea ice melt onset, freezeup, and melt season length. *Journal of Geophysical Research*, *114*, C12024. https://doi.org/10.1029/2009JC005436

Meredith, M. P., Stammerjohn, S. E., Venables, H. J., Ducklow, H. W., Martinson, D. G., Iannuzzi, R. A., et al. (2017). Changing distributions of sea ice melt and meteoric water west of the Antarctic Peninsula. *Deep Sea Research Part II: Topical Studies in Oceanography*, *139*, 40–57. https://doi.org/10.1016/j.dsr2.2016.04.019

Meredith, M. P., Venables, H. J., Clarke, A., Ducklow, H. W., Erickson, M., Leng, M. J., et al. (2013). The freshwater system west of the Antarctic Peninsula: Spatial and temporal changes. *Journal of Climate*, *26*(5), 1669–1684. https://doi.org/10.1175/JCLI-D-12-00246.1

Östlund, H. G., & Hut, G. (1984). Arctic Ocean water mass balance from isotope data. *Journal of Geophysical Research*, *89*(C4), 6373–6381. https://doi.org/10.1029/JC089iC04p06373

Parkinson, C. L., & DiGirolamo, N. E. (2016). New visualizations highlight new information on the contrasting Arctic and Antarctic sea-ice trends since the late 1970s. *Remote Sensing of Environment*, *183*, 198–204. https://doi.org/10.1016/j.rse.2016.05.020

Perovich, D. K., Grenfell, T. C., Light, B., Elder, B. C., Harbeck, J., Polashenski, C., et al. (2009). Transpolar observations of the morphological properties of Arctic sea ice. *Journal of Geophysical Research*, *114*, C00A04. https://doi.org/10.1029/2008JC004892

Perovich, D. K., Light, B., Eicken, H., Jones, K. F., Runciman, K., & Nghiem, S. V. (2007). Increasing solar heating of the Arctic Ocean and adjacent seas, 1979–2005: Attribution and role in the ice-albedo feedback. *Geophysical Research Letters*, *34*, L19505. https://doi.org/10.1029/2007GL031480

Petrich, C., Eicken, H., Polashenski, C. M., Sturm, M., Harbeck, J. P., Perovich, D. K., & Finnegan, D. C. (2012). Snow dunes: A controlling factor of melt pond distribution on Arctic sea ice. *Journal of Geophysical Research*, *117*, C09029. https://doi.org/10.1029/2012JC008192

Phillips, D. L., & Gregg, J. W. (2001). Uncertainty in source partitioning using stable isotopes. *Oecologia*, *127*(2), 171–179. https://doi.org/10.1007/s004420000578

Phillips, F. M., Mills, S., Hendrickx, M. H., & Hogan, J. (2003). Environmental tracers applied to quantifying causes of salinity in arid-region rivers: Results from the Rio Grande Basin, southwestern USA. In *Developments in water science* (Vol. 50, pp. 327–334). Netherlands: Elsevier. https://doi.org/10.1016/S0167-5648(03)80029-1

Polashenski, C., Golden, K. M., Perovich, D. K., Skyllingstad, E., Arnsten, A., Stwertka, C., & Wright, N. (2017). Percolation blockage: A process that enables melt pond formation on first year Arctic sea ice. *Journal of Geophysical Research: Oceans*, *122*, 413–440. https://doi.org/10.1002/2016JC011994

Polashenski, C., Perovich, D., & Courville, Z. (2012). The mechanisms of sea ice melt pond formation and evolution. *Journal of Geophysical Research*, *117*, C01001. https://doi.org/10.1029/2011JC007231

Rösel, A., Itkin, P., King, J., Divine, D., Wang, C., Granskog, M. A., et al. (2018). Thin sea ice, thick snow, and widespread negative freeboard observed during N-ICE2015 north of Svalbard. *Journal of Geophysical Research: Oceans*, *123*, 1156–1176. https://doi.org/10.1002/2017JC012865

Rösel, A., & Kaleschke, L. (2012). Exceptional melt pond occurrence in the years 2007 and 2011 on the Arctic sea ice revealed from MODIS satellite data. *Journal of Geophysical Research*, *117*, C05018. https://doi.org/10.1029/2011JC007869

Screen, J. A., & Simmonds, I. (2010). The central role of diminishing sea ice in recent Arctic temperature amplification. *Nature*, *464*(7293), 1334–1337. https://doi.org/10.1038/nature09051

Serreze, M. C., & Francis, J. A. (2006). The Arctic amplification debate. *Climatic Change*, *76*(3–4), 241–264. https://doi.org/10.1007/s10584-005-9017-y

Skrzypek, G., & Ford, D. (2014). Stable isotope analysis of saline water samples on a cavity ring-down spectroscopy instrument. *Environmental Science & Technology*, *48*(5), 2827–2834. https://doi.org/10.1021/es4049412

Smith, I. J., Eicken, H., Mahoney, A. R., Van Hale, R., Gough, A. J., Fukamachi, Y., & Jones, J. (2016). Surface water mass composition changes captured by cores of Arctic land-fast sea ice. *Continental Shelf Research*, *118*, 154–164. https://doi.org/10.1016/j.csr.2016.02.008

Souchez, R., Jouzel, J., Lorrain, R., Sleewaegen, S., Stiévenard, M., & Verbeke, V. (2000). A kinetic isotope effect during ice formation by water freezing. *Geophysical Research Letters*, *27*(13), 1923–1926. https://doi.org/10.1029/2000GL006103

Steen-Larsen, H. C., Sveinbjörnsdottir, A. E., Jonsson, T., Ritter, F., Bonne, J. L., Masson-Delmotte, V., et al. (2015). Moisture sources and synoptic to seasonal variability of North Atlantic water vapor isotopic composition. *Journal of Geophysical Research: Atmospheres*, *120*, 5757–5774. https://doi.org/10.1002/2015JD023234

Stenni, B., Masson-Delmotte, V., Selmo, E., Oerter, H., Meyer, H., Röthlisberger, R., et al. (2010). The deuterium excess records of EPICA Dome C and Dronning Maud Land ice cores (East Antarctica). *Quaternary Science Reviews*, *29*(1–2), 146–159. https://doi.org/10.1016/j.quascirev.2009.10.009

Sturm, M., & Massom, R. A. (2010). Snow and sea ice. In D. N. Thomas & G. S. Dieckmann (Eds.), *Sea ice* (2nd ed., pp. 153–204). Oxford, UK: Wiley-Blackwell. https://doi.org/10.1002/9781444317145.ch5

Thomson, J., Ackley, S., Shen, H. H., & Rogers, W. E. (2017). The balance of ice, waves, and winds in the Arctic autumn. *Eos*, *98*. https://doi.org/10.1029/2017EO066029

Thomson, J., Ackley, S., Girard-Ardhuin, F., Ardhuin, F., Babanin, A., Boutin, G., et al. (2018). Overview of the Arctic sea state and boundary layer physics program. *Journal of Geophysical Research: Oceans*, *123*. https://doi.org/10.1002/2018JC013766

Tschudi, M. A., Stroeve, J. C., & Stewart, J. S. (2016). Relating the age of Arctic sea ice to its thickness, as measured during NASA's ICESat and IceBridge campaigns. *Remote Sensing*, *8*(6), 457. https://doi.org/10.3390/rs8060457

Walker, S. A., Azetsu-Scott, K., Normandeau, C., Kelley, D. E., Friedrich, R., Newton, R., et al. (2016). Oxygen isotope measurements of seawater ($H_2{}^{18}O/H_2{}^{16}O$): A comparison of cavity ring-down spectroscopy (CRDS) and isotope ratio mass spectrometry (IRMS). *Limnology and Oceanography: Methods*, *14*(1), 31–38. https://doi.org/10.1002/lom3.10067

Webster, M. A., Rigor, I. G., Perovich, D. K., Richter-Menge, J. A., Polashenski, C. M., & Light, B. (2015). Seasonal evolution of melt ponds on Arctic sea ice. *Journal of Geophysical Research: Oceans*, *120*, 5968–5982. https://doi.org/10.1002/2015JC011030

Weeks, W. F., & Ackley, S. F. (1986). The growth, structure, and properties of sea ice. In N. Untersteiner (Ed.), *The geophysics of sea ice* (pp. 9–164). Boston, MA: Springer. https://doi.org/10.1007/978-1-4899-5352-0_2

Yuan, F., Sheng, Y., Yao, T., Fan, C., Li, J., Zhao, H., & Lei, Y. (2011). Evaporative enrichment of oxygen-18 and deuterium in lake waters on the Tibetan Plateau. *Journal of Paleolimnology*, *46*(2), 291–307. https://doi.org/10.1007/s10933-011-9540-y

Zhao, H., Xu, B., Yao, T., Wu, G., Lin, S., Gao, J., & Wang, M. (2012). Deuterium excess record in a southern Tibetan ice core and its potential climatic implications. *Climate Dynamics*, *38*(9–10), 1791–1803. https://doi.org/10.1007/s00382-011-1161-7